

1 Effect of water depth and swell parameters on 2 wave propagation in the coastal zone of Benin

3
4
5
6

7 ABSTRACT

8

The coastal zone is studied as a morphodynamic system in the present work. A morphodynamic system comprises a geomorphological entity that adjusts its morphology in response to variations in a dynamic component. In recent years, particularly from 2015 to 2016, strong swells have been observed and have induced the destruction of coastal infrastructure and strong coastal erosion in the Gulf of Guinea, particularly Benin. Following this observation, our study is carried out to understand the origin of these strong events. Through this work, we tried to highlight the effect of water depth and swell parameters on wave propagation using experimental models from the literature. For this reason, MATLAB and Mathematica software were used for simulations. It can be said from the results obtained that the wave height has a considerable effect on the wave profile. The variation in water depth as a function of distance from the bed shows that it significantly affects the wave and its components.

9

10 **Keywords:** Wave simulation; Water depth; Swell and Wave propagation; Benin coastal zone

11

12 SCIENTIFIC NOTATION TABLES

13 v : Ocean water flow Velocity (m/s) ;

14 ρ : Density of sea water (kg/m³) ;

15 Φ : Velocity potential in the ocean (m²/s) ;

16 η : Vertical elevation of the water level relative to the reference (m) ;

17 β : Inclination of the seabed relative to the horizontal (rad) ;

18 Υ : Hydrodynamic pressure (Pa) ;

19 g : Acceleration of gravity (m/s²) ;

20 H : Crest-to-trough height of the swell (m) ;

21 H_0 : Crest-to-trough height of the offshore swell (m) ;

22 H_d : Crest-to-trough height of the swell at the breaking point (m) ;

23 H_s : Significant crest-to-trough swell height (m) ;

24 H_{max} : Maximum crest to trough height of the swell (m) ;

25 H_{min} : Minimum crest-to-trough wave height (m) ;

26 T_m : Average swell period (s) ;

27 T_p : Peak wave period (s) ;

28 $L = \frac{2\pi}{k}$: Wavelength of the swell (m) ;

29 $T = \frac{2\pi}{\omega}$: Swell period (s) ;

30 d : Near sea surface-bottom distance in coastal zones (m) ;

31 \vec{r} : Position vector of a point located on the free surface;

32 V_g : Group swell Velocity (m/s) ;

33 V_ϕ : Swell phase Velocity (m/s) ;

34 V_x : Horizontal Velocity of the water particles struck by the swell;

35 V_z : Vertical Velocity of the water particles struck by the swell;

36 K_R : Refraction coefficients;
37 K_S : Shoaling coefficients;
38 A_x : Horizontal accelerations of water particles struck by the swell;
39 A_z : Vertical acceleration of water particles struck by the swell;
40 \mathcal{L}_x : Horizontal movement of water particles struck by the swell;
41 \mathcal{L}_z : Vertical movement of water particles hit by the swell;;
42 MCA : Millenium Challenge Account.

43
44

45 1. INTRODUCTION

46 Comprehensive theoretical research on the propagation of waves in Benin's coastal
47 areas could yield vital information for the region's coastal risk management and planning. [1].
48 The study of swell and wave propagation in the coastal zone of Benin involves
49 understanding various factors that influence wave behavior, such as wind patterns, local
50 water depth, coastal morphology, fetch, tide, ocean currents, and oceanographic
51 conditions[2]. A theoretical study typically involves mathematical modeling and simulation to
52 predict wave characteristics along the coast of Benin. Studying the ocean as a whole
53 requires bridges linking the transversal skills of the different sciences in this case theoretical
54 physics through modeling and analysis which lead to understanding and the search for
55 solutions to the consequences of the increase in the level of the sea[1]. Mathematical
56 theories, at the basis of all theoretical knowledge of the physical functioning of our
57 environment, which deal with waves, have developed and become more complex. They
58 represent many phenomena linked to waves based on hypotheses developed from the
59 general equations of fluid mechanics, and now make it possible to study ever more
60 sophisticated problems analytically and numerically[3]. Overall, a theoretical study on swell
61 and wave propagation in the coastal zone of Benin requires a multidisciplinary approach
62 integrating oceanography, meteorology, hydrodynamics, and coastal engineering to provide
63 valuable information for coastal management and decision-making[4]. The most spectacular
64 physical manifestation occurring in the ocean is undoubtedly the swell. The coastline of
65 Benin has suffered severe erosion for several years[5]. This phenomenon could be
66 explained by a hydrodynamic dominated mainly by swells generated by the winds as well as
67 a sandy coastline subject to a local microtidal type tide and a seasonal evolution of the
68 intensity of the swells. In short, the coast of Cotonou in Benin is subject to two swell regimes:
69 short swells (less energetic) generated by local winds and long swells (very energetic)
70 generated in the South Atlantic which are the engine of one of the most significant coastal
71 drifts in the world, from west to east[6]. In Cotonou, coastal transit is caused by the oblique
72 attack of north-east or east-north-east swells during different storms [5]. Under the action of
73 currents, winds, or swells, the solid particles, that form the sediments encountered in rivers
74 and along coastlines, can be torn from the seabed, suspended, or transported over
75 distances. More or less large and deposited in calm areas. These interactions are extremely
76 complex in nature and the sedimentary movements that can be observed depend on multiple
77 parameters. Velocity gradients in the fluid, vortices, bottom geometry, bank lines, nature of
78 materials, thickness on the bedrock, porosity, and cohesion of the deposits, characteristics
79 of the fluid... Will intervene in the conditions of erosion and transport of the materials. All
80 these parameters, in addition, will not be constant over time but will undergo fluctuations.
81 The swell in the fluid mass will cause the sediments to flow in certain situations in a mass
82 direction toward privileged sectors due to reactions from translational and compensatory
83 currents, return currents, orbital movements on the seabed, and coastal or return currents.
84 On the sea surface, the friction of the local wind causes the water surface to move and
85 generate ripples[1], [7]. This 'sea of wind' is the superposition of several sinusoidal waves,
86 forming 'irregular' waves[2], [4]. Under the effect of pressure gradients associated with
87 gravity and induced by these variations in water height, these waves then propagate and are

88 called gravity waves, or surface waves. These waves turn into swells when they propagate.
89 The swell is thus the part of the sea state characterized by its absence of a relationship with
90 the local wind. As part of this study, no distinction will be made between swell and waves,
91 these two terms will define the sea state arriving on the shore. The land-sea interface is an
92 extremely fragile environment. Coastlines, interfaces between land and sea, are places of
93 great biological and landscape diversity, subject to strong pressures from natural elements
94 and human beings. In the coastal zone, the most dynamic zones are the internal surf and
95 swash zones[5]. The swash zone is of fundamental importance in the study of the coastal
96 zone. The internal surf zone thus represents the border between the emerged part of the
97 beach and the breaking zone. The internal surf zone and the swash zone thus form the very
98 last zone of the beach where the waves will dissipate or reflect their remaining energy[1],
99 [8]. Throughout the world, coastlines are threatened by the combination of a multitude of
100 factors, sometimes natural and most often anthropogenic. Thus, to the local disturbances
101 caused to coastal areas by port infrastructures, dams, sediment collection from the beach, or
102 even urban expansion, are added the global consequences of climate change, including the
103 certain rise in the level of oceans and the probable amplification of devastating marine
104 weather conditions. The direct consequence of global warming, the rise in ocean levels will
105 have obvious consequences on coastal erosion in the decades to come. It is thus estimated,
106 on a global scale, that sea levels could rise between 10 and 25 cm over the last century and
107 28 and 98 cm by 2100 according to estimates from the IPCC (Intergovernmental Panel on
108 Climate Change). Climate change presented in their ar5 assessment report, based on
109 different warming scenarios (IPCC, 2014)[1], [8]. In Cotonou, since 2011, it was recently
110 calculated that the average increase in sea level was 3.2 mm year⁻¹, which is close to the
111 global values obtained over a similar period (IPCC, 2014)[9]. The simplest mathematical
112 representation assuming the water waves used for the simulation is given as follows: two-
113 dimensional (2-D), small amplitude, sinusoidal, and progressively definable by their
114 amplitude and wave period in a depth of water given. In the simple representation of
115 swells/waves, the movements and displacements of swell/wave, the kinematics (i.e.,
116 velocities and accelerations of swell/wave), and the dynamics (i.e. (i.e., wave/wave pressure
117 and resultant forces and moments) are determined for technology design evaluations. When
118 the wave amplitude becomes larger, simple treatment cannot be scaled. For regular
119 swell/wave, we consider the 2-D approximation of the ocean surface deviated from a pure
120 sinusoid [8]. This representation requires more complicated mathematical theories. These
121 theories become non-linear and allow the formulation of swells/waves that are not sinusoidal
122 in shape; for example, flat troughs and sharp ridges in shallow water when swells/waves are
123 relatively high. The simplest swell/wave theory is first order and small amplitude, or the airy
124 theory which is called the linear theory[3]. This representation requires more complicated
125 mathematical theories.

126

127 **2. MATERIAL AND METHODS**

128 **2.1 Presentation of the study site**

129



Figure 1a: Geographical location of the coastal zone of Benin in the Gulf of Guinea

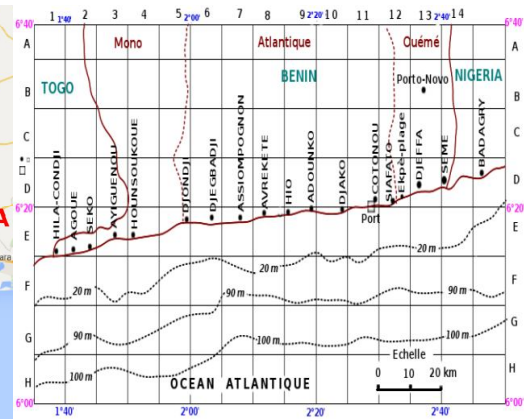


Figure 1b: Bathymetric map of the Benin coastal zone



Figure 1c: Image of Benin's coastal strip

130
131
132
133
134
135
136
137
138
139
140
141
142
143
144
145
146
147
148
149

The coastal zone of Benin, between $6^{\circ}15'$ and $6^{\circ}38'$ north latitude, is part of the coastal sedimentary basin, the oldest of which dates back to the Cretaceous. Benin is a coastal state in the Gulf of Guinea (**figure 1a**). The coastline generally presents weak concavities oriented towards the ocean on this coast. There is increasing erosion towards the east. The climate is subequatorial with two dry seasons and two rainy seasons [4], [8], [10].

In the coastal zone of Benin, there is no major obstacle that could significantly modify the direction of wave propagation ($\theta \approx \theta_0$) [8]. The average slope in the shoaling zone on this site is $p = \tan\beta \approx \frac{90}{2000} = 0,045$ [2] (**Figure 1b**). In Benin, the swells which propagate towards the coast have a period T which varies between 10 s and 14 s and whose peak period is $T_p = 11.50\text{ s}$. Experimental measurements have shown that these waves break at the point of local depth d_b such that $4\text{ m} \leq d_b \leq 5\text{ m}$ and that their period oscillates between 9 s and 15 s [11]. Their heights vary almost sinusoidally and have two maxima and two minima on the same day. These heights vary between 0.6 m and 1.4 m . The maxima are observed around 5 a.m and 5 p.m GMT and the minima around 00 a.m and 12 p.m [12]. From data measurements relating to swell carried out at the autonomous port of Cotonou, at time intervals of five minutes over four consecutive years (June 2015 to April 2016) and obtained from the Institute of Fisheries and Oceanographic Research of Benin (IRHOB) of the Beninese Center for Scientific and Technical Research (CBRST), we have:

- Performs analysis of wave statistics on the coast of Benin.

- 150 ➤ Simulated the temporal evolution of wave parameters such as the significant height H_s (m),
 151 the period of the peak T_p (s) and the direction of the peak Dir (°).
 152 ➤ Shown the evolution of the vertical elevation η of the sea surface as a function of local water
 153 depth and compare swell profiles as a function of time in the different areas. For the study of
 154 swell propagation on this site, the abscissa axis is oriented in the East-West direction and the
 155 ordinate axis in the North-South direction as shown in **Figure 2** below:

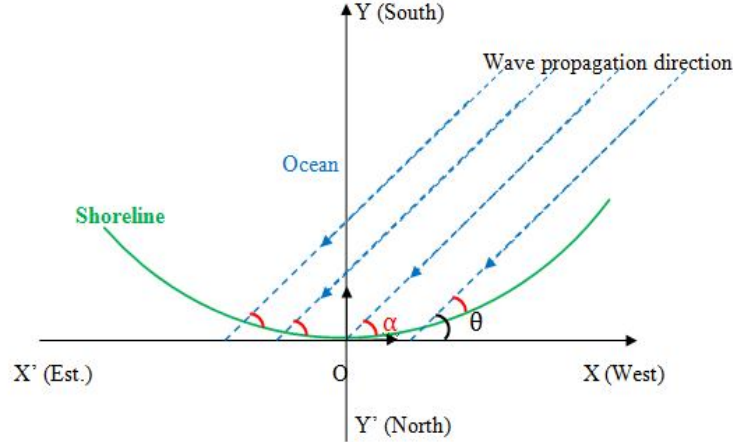


Figure 2: Schematization of the study benchmark and direction of wave propagation in Benin coastal zone.

156
 157 The coastal strip of Benin is oriented in the South-West-West direction and thus tilts at an
 158 angle $\theta_o = 20^\circ$ approximately about the West-East direction [4].
 159

2.2. Equations to solve the problem

- The movement of fluids (air and ocean) obeys the following Navier-Sokes equation [7].

$$162 \frac{\partial \vec{v}_i}{\partial t} + (\vec{v}_i \cdot \nabla) \vec{v}_i + \frac{1}{\rho_i} (\nabla P_i) - \vec{g} - \frac{\mu}{\rho_i} (\nabla^2 \vec{v}_i) = \mathbf{0} \text{ with } i = 1, 2 \quad (1)$$

163 Irrotational and incompressible coastal flow can be modeled using Euler's equations in 3
 164 dimensions. The strong non-linear nature of these equations prevents us from directly applying a
 165 numerical solution method. We must therefore simplify them before applying a numerical
 166 scheme. The viscosity in these two media being very negligible [13] and for surface waves, the
 167 convective term is negligible ($\mu \ll \rho_i$) compared to the acceleration $(\vec{v}_i \cdot \nabla) \vec{v}_i \ll \frac{\partial \vec{v}_i}{\partial t}$ [1].

168 The oceanic environment is an incompressible fluid ($div(\vec{v}) = 0$), the flow is potential ($\vec{v} = \vec{\nabla} \phi$)
 169 and for a perfect fluid, we show that an irrotational disturbance remains so indefinitely. We can
 170 apply this theorem to the movement of waves whose flow will be assumed to be zero rotational
 171 (irrotational) $\text{rot}(\vec{v}) = \vec{0}$ [1] where \vec{v} is the speed of a water particle driven by the flow and $\phi_2 = \phi$ the
 172 scalar potential of the velocities in the ocean and ϕ_1 that of the atmosphere. Thus, we obtain the
 173 Laplace equation below [14] $\Delta \phi = 0$. The solution of equation (1) allows us to find the dynamic
 174 pressure Y [15].

$$175 \mathbf{Y} = -\rho \left(\frac{\partial \phi}{\partial t} \right) \quad (2)$$

- The area in which the effect of the Airy or Stokes swell (swell of very small amplitude compared to their wavelength) is felt is such [15], [16].

$$178 \begin{cases} -\infty \leq x \leq +\infty \\ -\infty \leq y \leq +\infty \\ -d \leq z \leq 0 \end{cases} \quad (3)$$

- A water particle at a point on the free surface has a vertical speed $v_z = \frac{\partial \eta}{\partial t}$ along the vertical axis. The kinematic condition in $z = \eta$ gives [7].

$$181 \quad \left(\frac{\partial \phi}{\partial z}\right)_{(z=\eta)} = \left(\frac{\partial \phi_i}{\partial z}\right)_{(z=\eta)} = \frac{\partial \eta}{\partial t} \quad (4)$$

182 • The swell being a surface wave, its effect disappears after a certain depth ($z = -d$). The
183 condition of non-penetration to the bottom amounts to [2], [8].

$$184 \quad v_z(z = -d) = 0 \Rightarrow \left(\frac{\partial \phi}{\partial z}\right)_{(z=-d)} = 0 \quad (5)$$

185 • The dynamic condition at $z = \eta$ due to the existence of pressure and gravity forces at
186 altitude z is written [15], [16].

$$187 \quad \left[g\eta + \frac{\partial \phi}{\partial t} \right]_{z=0} = 0 \Rightarrow \left[\frac{\partial^2 \phi}{\partial t^2} + g \frac{\partial \phi}{\partial z} \right]_{z=0} = 0 \quad (6)$$

188 • The direction of wave propagation is almost rectilinear. It is assimilated to the axis (O, \vec{i}) and
189 the average vertical elevation of the free surface is zero over a period.

$$190 \quad \int_t^{t+T} \eta(\vec{r}, t) dt = \int_x^{x+L} \eta(\vec{r}, t) dx = 0 \quad (7)$$

191 • Any swell of wavelength propagates through three particular zones [16], [17]. Offshore
192 (deep water) when $d > \frac{L}{2}$; the lifting zone (Shoaling zone) if $\frac{L}{25} \leq d \leq \frac{L}{2}$; the breaking zone or
193 shallow waters (Surf and Swash zones) for $0 \leq d \leq \frac{L}{25}$

194 • On the Beninese coast, the average slope in the Shoaling zone [2], [12] is :

$$195 \quad p = \tan(\beta) = \frac{90}{2000} = 0,045 \quad (8)$$

196 According to the bathymetric map along the Beninese maritime coast (**Figure 2b**) shows us that
197 there is very little variation in the wavelength of the swells, either:

$$198 \quad L = \frac{2\pi}{k} = \frac{gT^2}{2\pi} \quad (9)$$

199 **2.3. Expression of $\phi(\vec{r}, t)$, $\eta(\vec{r}, t)$ and the group velocity V_g**

200 Solving equation (1) with conditions (3), (4), (5) and (6) gives complex results of which only
201 the real parts below reflect the physical phenomenon [18], [19].

$$202 \quad \begin{cases} \phi_1 = \phi_1(x, y, z, t) = \frac{gH}{2w} e^{kz} \sin(\vec{k} \cdot \vec{r} - \omega t) \\ \phi_1 = \phi_1(x, y, z, t) = \frac{gH \cosh[k(z+d)]}{2w \cosh(kd)} \sin(\vec{k} \cdot \vec{r} - \omega t) \\ \eta = \eta(x, y, t) = \eta_0 \cos(\vec{k} \cdot \vec{r} - \omega t) = \frac{H}{2} \cos(\vec{k} \cdot \vec{r} - \omega t) \\ Y = -\rho \frac{\partial \phi}{\partial t} = \frac{\rho g H \cosh[k(z+d)]}{2 \cosh(kd)} \cos(\vec{k} \cdot \vec{r} - \omega t) \end{cases} \quad (10)$$

203 The fluid velocity in the x direction is: $V_x = \frac{\partial \phi}{\partial x}$ and the fluid velocity in the z direction is: $V_z = \frac{\partial \phi}{\partial z}$.

204 The positions, velocities and accelerations of local fluids are:

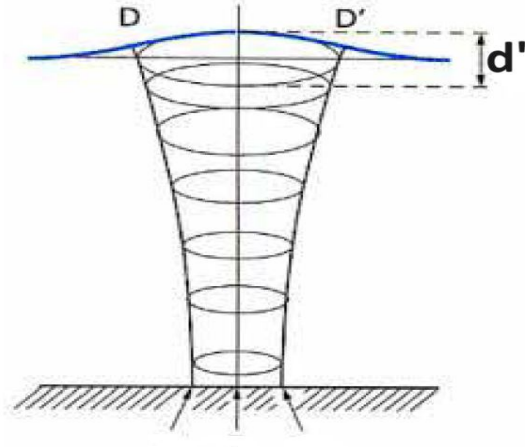
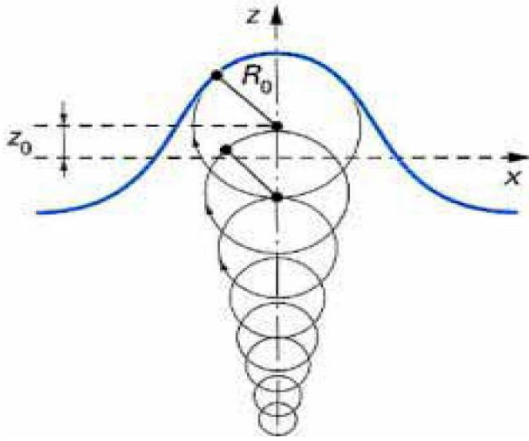
$$205 \quad \vec{V} \begin{cases} V_x = \frac{gHT}{2L} \frac{\cosh[2\pi(z+d)/L]}{\cosh(2\pi d/L)} \cos(\theta) \\ V_z = \frac{gHT}{2L} \frac{\sinh[2\pi(z+d)/L]}{\cosh(2\pi d/L)} \sin(\theta) \end{cases} \text{ with } \theta = \frac{2\pi x}{L} - \frac{2\pi t}{T} \quad (11)$$

206 The integration of this equation (11) gives the equations that parameterize the position of a water
207 particle struck by the swell.

$$208 \quad \vec{OM} \begin{cases} X = \frac{H}{2} \frac{\cosh[2\pi(z+d)/L]}{\cosh(2\pi d/L)} \sin(\theta) \\ Z = \frac{H}{2} \frac{\sinh[2\pi(z+d)/L]}{\cosh(2\pi d/L)} \cos(\theta) \end{cases} \text{ with } \theta = \frac{2\pi x}{L} - \frac{2\pi t}{T} \quad (12)$$

209 These equations express water particles' velocity and position components at any
210 distance $(z + d)$ above the bottom. They are periodic in x and t . For a given value of the phase
211 angle $\theta = 2\pi \left(\frac{x}{L} - \frac{t}{T} \right)$. The trajectory of the particles is therefore circular in infinite depth
212 (offshore) and elliptical in shape that becomes more and more crushed as the bottom rises. The
213 equations of system (11) generally parameterize the ellipses with major horizontal axis DD' and
214 minor vertical axis d' verifying the equation:

215 $\left(\frac{x}{DD'}\right)^2 + \left(\frac{z}{d'}\right)^2 = 1$ with $\begin{cases} DD' = \frac{H \cosh[2\pi(z+d)/L]}{2 \cosh(2\pi d/L)} \\ d' = \frac{H \sinh[2\pi(z+d)/L]}{2 \cosh(2\pi d/L)} \end{cases}$ (13)



216 **Figure 3a:**Trajectory of water particles in Gerstner swell [20], [21] **Figure 3b:**Trajectory of water particles in Stokes swell [21], [21]

216

217 This model established in 1804 by Gerstner is a rigorous solution for a fluid at infinite depth
218 (**Figure 3a**). Each fluid particle is supposed to rotate around a point with coordinates X_0, Z_0 ,
219 describing a circumference of radius R , decreasing exponentially with depth d .

220 The derivation of this equation (11) gives the equations that parameterize the accelerations of the
221 particles of the fluid struck by the swell. The accelerations of the fluid particles are:

222
$$\begin{cases} A_x = \frac{g\pi H \cosh[2\pi(z+d)/L]}{L \cosh(2\pi d/L)} \sin(\theta) \\ A_z = -\frac{g\pi H \sinh[2\pi(z+d)/L]}{L \cosh(2\pi d/L)} \cos(\theta) \end{cases} \text{ with } \theta = \frac{2\pi x}{L} - \frac{2\pi t}{T} \quad (14)$$

223 And the movement of water particles is given by:

224
$$\begin{cases} \mathcal{L}_x = -\frac{HgT^2 \cosh[2\pi(z+d)/L]}{4\pi L \cosh(2\pi d/L)} \sin(\theta) \\ \mathcal{L}_z = \frac{HgT^2 \sinh[2\pi(z+d)/L]}{4\pi L \cosh(2\pi d/L)} \cos(\theta) \end{cases} \text{ with } \theta = \frac{2\pi x}{L} - \frac{2\pi t}{T} \quad (15)$$

225 The secondary external pressure under a wave is the sum of two pressure components,
226 dynamic and static, and is given by:

227
$$Y' = \frac{\rho g H \cosh[2\pi(z+d)/L]}{2 \cosh(2\pi d/L)} \cos(\theta) - \rho g z + p_0 \text{ with } \theta = \frac{2\pi x}{L} - \frac{2\pi t}{T} \quad (16)$$

228 The equation for the water surface is given by:

229
$$\eta = \eta_1 + \eta_2 = \frac{H}{2} \cos\left(\frac{2\pi x}{L_1} - \frac{2\pi t}{T_1}\right) + \frac{H}{2} \cos\left(\frac{2\pi x}{L_2} - \frac{2\pi t}{T_2}\right) \quad (17)$$

230 and

231
$$\eta_{enveloppe} = \pm H \cos\left[\pi \left(\frac{L_2 - L_1}{L_1 L_2}\right) x - \pi \left(\frac{T_2 - T_1}{T_1 T_2}\right) t\right] \quad (18)$$

232 The swell dispersion relation according to the linear theory[22], [23] is :

233
$$\omega^2 = gk \tanh(kd) \quad (19)$$

234 The phase (celerity) and group velocities of a swell are respectively[17], [24].

235
$$\begin{cases} V_\varphi = \frac{\omega}{k} = \sqrt{\frac{g}{k} \tanh(kd)} \\ V_g = \frac{\partial \omega}{\partial k} = \frac{1}{2} \frac{\omega}{k} \left(1 + \frac{2kd}{\sinh(2kd)}\right) \end{cases}$$

236 (20)

237 Note that an argument of the hyperbolic tangent $kd = 2\pi d/L_0$ is large, the
 238 $\tanh(kd)$ approaches 1, and for small values of kd , $\tanh(kd) \simeq kd$. Water waves are classified in
 239 Table 1 based on the relative depth criterion d/L_0 .
 240

Classification	$\mu = d/L_0$	kd	$\tanh(kd)$
Deep Waters	1/2 to $+\infty$	π to $+\infty$	= 1
Shoaling zone	1/25 to 1/2	$\pi/10$ to π	$\tanh(kd)$
Shallow waters	0 to 1/25	0 to $\pi/10$	= kd

241 **Tableau 1** :Waves classification

242 > In deep waters, $V_{g_0} = \frac{1}{2}V_\varphi = \frac{gT}{4\pi} \text{gold} L_0 = \frac{gT^2}{2\pi}$ [25];

243 > In the Shoaling zone, $V_g = \frac{1}{2} \left(1 + \frac{2kd}{\sinh(2kd)} \right) \sqrt{\frac{g}{k} \tanh(kd)}$;

244 > In the shallow waters, $V_g = V_\varphi = \sqrt{gd}$ [26];

245 In the end, we have:

$$246 \quad V_g(d) = \begin{cases} \frac{gT}{4\pi} \text{ if } \frac{d}{L_0} > \frac{1}{2} \\ \frac{1}{2} \left(1 + \frac{2kd}{\sinh(2kd)} \right) \sqrt{\frac{g}{k} \tanh(kd)} \text{ if } \frac{1}{25} \leq \frac{d}{L_0} \leq \frac{0}{2} \\ \sqrt{gd} \text{ if } 0 \leq \frac{d}{L_0} \leq \frac{1}{25} \end{cases} \quad (21)$$

247 Gold by posing $k = 2\pi/L_0$

$$248 \quad V_g(d) = \begin{cases} \frac{gT}{4\pi} \text{ if } \frac{d}{L_0} > \frac{1}{2} \\ \frac{1}{2} \left(1 + \frac{4\pi d/L_0}{\sinh(4\pi d/L_0)} \right) \sqrt{\frac{gL_0}{2\pi} \tanh(2\pi d/L_0)} \text{ if } \frac{1}{25} \leq \frac{d}{L_0} \leq \frac{1}{2} \\ \sqrt{gd} \text{ if } 0 \leq \frac{d}{L_0} \leq \frac{1}{25} \end{cases} \quad (22)$$

249 2.4.Swellheight

250 In deep water, the swell height is constant and is $H = H_0 = cste$.
 251 In the Shoaling zone [7], [8], $H = K_S K_R H_0$ Where

$$252 \quad K_S = \sqrt{\frac{V_{g_0}}{V_g}} = \left(\frac{2\pi d/L_0}{\cosh^2(2\pi d/L_0)} + \tanh(2\pi d/L_0) \right)^{-\frac{1}{2}} \text{ and } K_R = \sqrt{\frac{\cos\theta_0}{\cos\theta}} \quad (23)$$

253 Are respectively the Shoaling and refraction coefficients, θ_0 and θ the directions of propagation of
 254 the wave before and after refraction. So we get, [12]:

$$255 \quad H = H_0 \sqrt{\frac{\cos\theta_0}{\cos\theta}} \left(\frac{2\pi d/L_0}{\cosh^2(2\pi d/L_0)} + \tanh(2\pi d/L_0) \right)^{-\frac{1}{2}}$$

256 (24)

257 The height of the swell decreases in the breaking zone [5], [21] and According to P.
 258 Bonneton (2002), this height is given by:

259 In the end, we have:

$$260 \quad H(d) = \begin{cases} H_0 \text{ if } \frac{d}{L_0} > \frac{1}{2} \\ H_0 \sqrt{\frac{\cos\theta_0}{\cos\theta}} \left(\frac{2\pi d/L_0}{\cosh^2(2\pi d/L_0)} + \tanh(2\pi d/L_0) \right)^{-\frac{1}{2}} \text{ if } \frac{d_b}{L_0} \leq \frac{d}{L_0} \leq \frac{1}{2} \\ H_0 \left[\frac{2H_0}{T \tan\beta \sqrt{gd_b}} \left(\frac{d}{d_b} \right)^{-1/2} + \left(1 - \frac{2H_0}{T \tan\beta \sqrt{gd_b}} \right) \left(\frac{d}{d_b} \right)^{1/4} \right]^{-1} \text{ if } 0 \leq d \leq d_b \end{cases} \quad (25)$$

261
 262
 263

264 **3. RESULTS AND DISCUSSION**

265 **3.1. Results Presentations**

266 > The curves in **Figure 4** reveal the temporal distribution of the hydrodynamic
 267 parameters of the port of Cotonou from 2015 to 2016. The data observed every hour of the
 268 parameters characterizing the state of the waves (significant height, peak direction, and peak
 269 period) at both anchorages from December 2015 to August 2016 are presented in **Figure 4**.

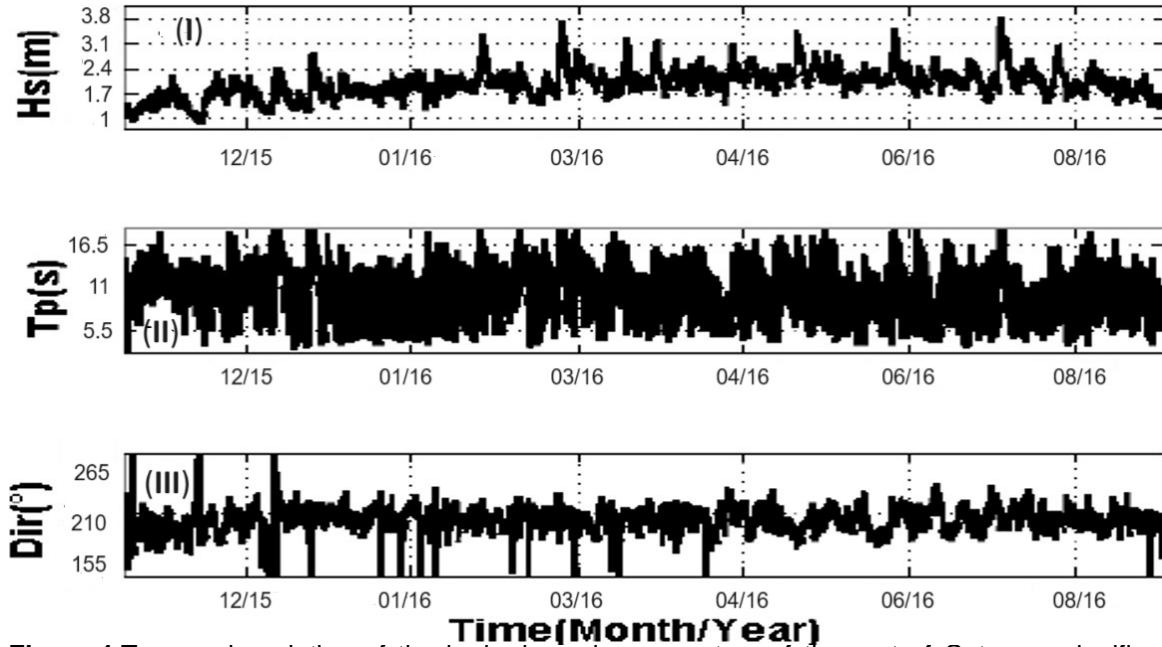


Figure 4: Temporal evolution of the hydrodynamic parameters of the port of Cotonou: significant wave height (Hs) (I), peak period (Tp) (II), and direction (Dir) (III) between 2015 and 2016.

270 > The following Figure 5 shows us the comparison of wave profiles and physical quantities as a
 271 function of time.
 272

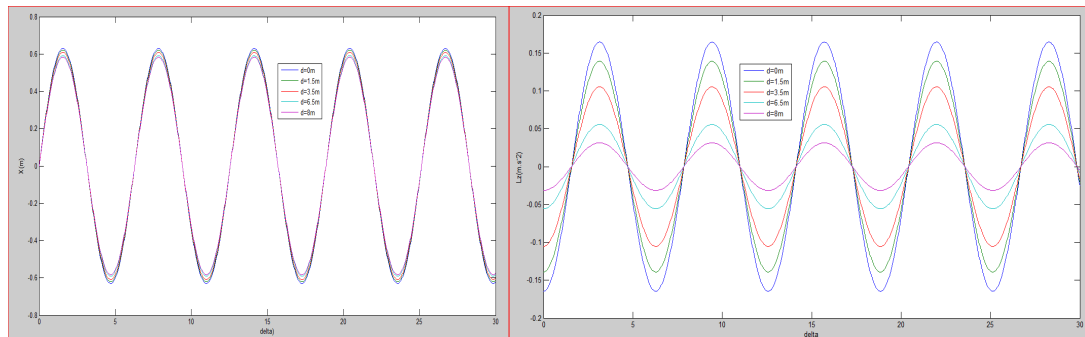


Figure 5a: Variation of horizontal position X **Figure 5b:** Variation of vertical position Z

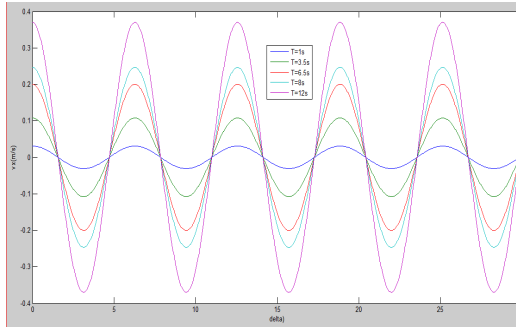


Figure 5c: Variation of the horizontal velocity of water particles

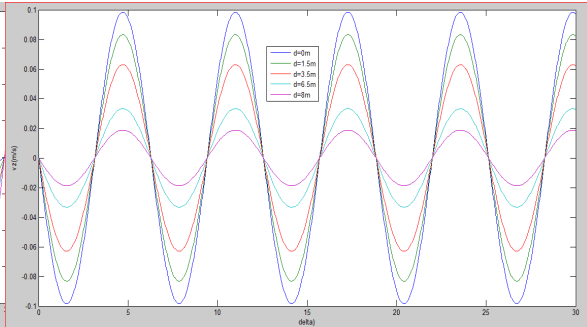


Figure 5d: Variation of the vertical velocity of water particles

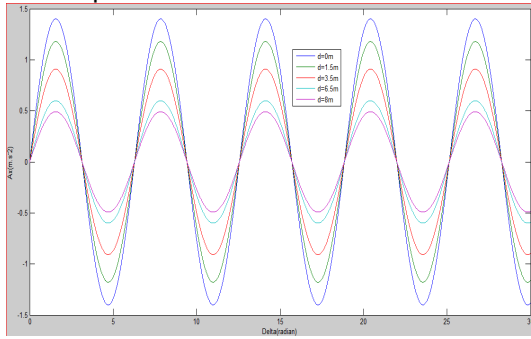


Figure 5e: Variation of horizontal acceleration of water particles

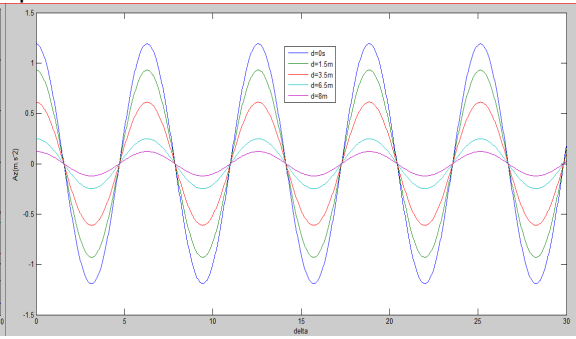


Figure 5f: Variation of vertical acceleration of water particles

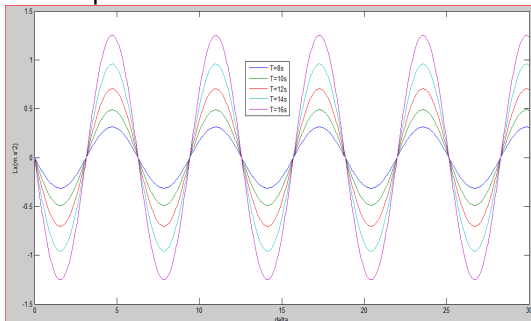


Figure 5g: Variation in horizontal displacement of water particles to $d=cst$

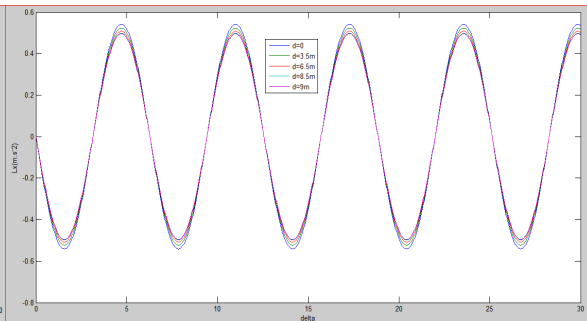


Figure 5h: Variation in horizontal displacement of water particles to $T=cst$

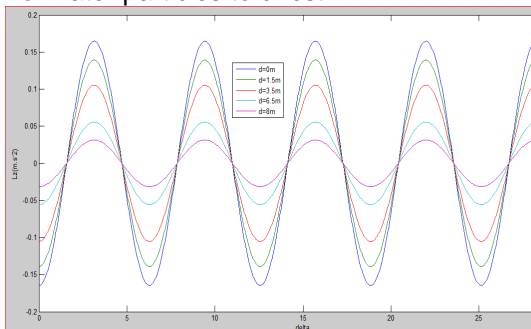


Figure 5i: Variation of vertical displacement of water particles

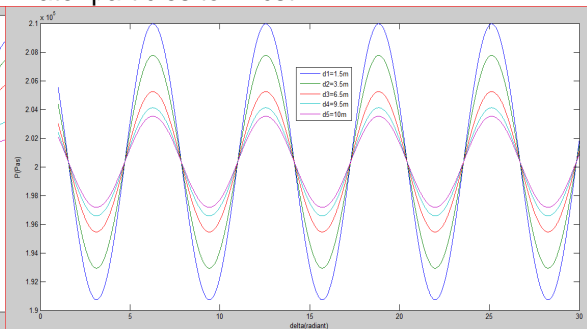
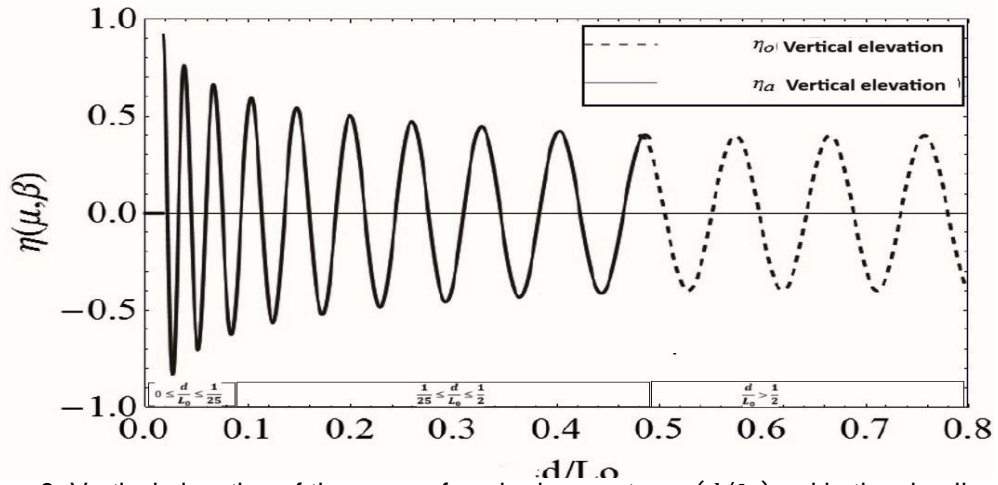


Figure 5j: Variation of dynamic pressure

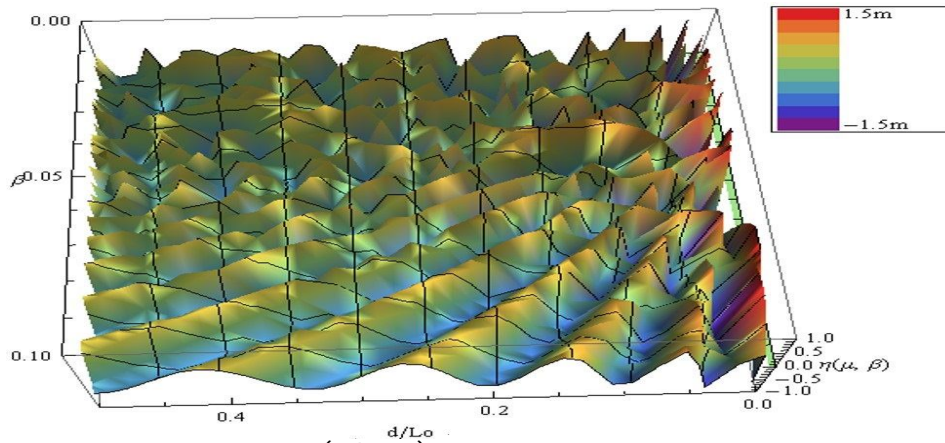
273
274
275

➤ **Figures 6,6a, and 6b,** show the evolution of the vertical elevation of the sea surface as a function of the local water depth μ and the slope of the seabed β . The curve in **Figure 6** is a

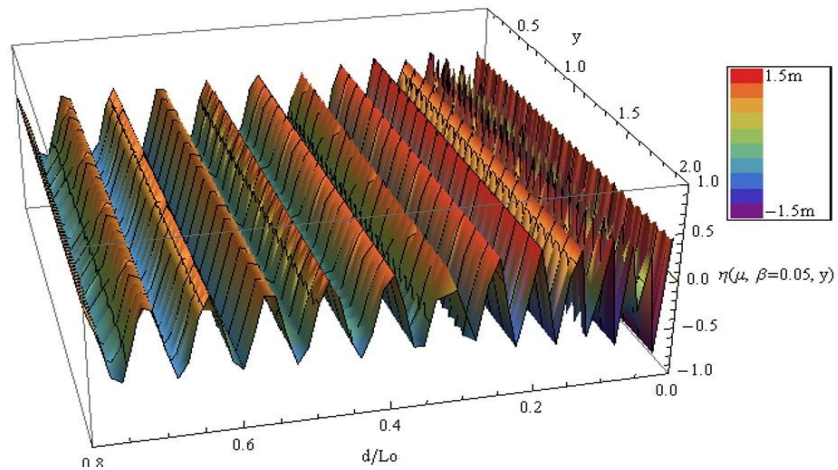
276 representation in dimension 2 (2D) whereas those of **Figures 6a** and **6b** are its representations in
 277 dimension 3 (3D).



278 **Figure 6:** Vertical elevation of the sea surface in deep water $\eta_0(d/L_0)$ and in the shoaling
 279 zone $\eta_a(d/L_0, \beta)$ in dimension two of the local water depth d/L_0 .
 280
 281



282 **Figure 6a:** Vertical elevation $\eta_a(d/L_0, \beta)$ of the sea surface in the shoaling zone in 3D as a
 283 function of the local water depth d/L_0 and the seabed slope β .
 284



285

286 **Figure 6b:** Vertical elevation of the marine surface offshore $\eta_o(d/L_0)$ and in the shoaling zone
287 $\eta_a(d/L_0, \beta = 0,05)$ in 3D of the local water depth d/L_0 .
288

289 **3.2. ANALYSIS AND DISCUSSION OF RESULTS**

290 ➤ It is important to note that the amplitude of the speed decreases exponentially with a
291 coefficient proportional to the wave number k . Therefore, the orbital speed of waves with a larger
292 period (smaller number of waves) will be more present at the bottom than that of waves with short
293 periods (**Figures 3a** and **3b**). The waves induce an orbital movement in the water and the
294 amplitude of this movement decreases with depth (**Figures 3a** and **3b**). In shallow water, the
295 elliptical paths followed by water particles flatten to horizontal lines, particularly at the bottom,
296 where there is no vertical flow. The trajectory of the particles is therefore circular in infinite depth
297 (offshore) and elliptical becomes more and more crushed as the bottom rises.

298 ➤ **Figure 4.I** indicate a strong temporal variability of H_s extending from typical wind force
299 values (minimum 0.71 m) to fairly energetic swells (maximum 3.22 m) during the years 2015 and
300 2016, some sequences exceptionally energetic with significant height values between 3.05 and
301 3.22 m. This mixture of ocean regime and sea wind is corroborated by the maximum swell periods
302 observed, varying between 5.50 and 15.66 s (**Figure 4.II**). The observed wave peak periods vary
303 between 4.38 and 17.85 s with an average of 11.7 s. The maximum direction of all waves varies
304 very little (standard deviation of 2.38°) with an average direction of 211.5° clockwise from the
305 north (dominant waves from the SSW sector) except on rare occasions (266 and 235° respectively
306 in 2015 and 2016, (**Figure 4.III**, we see a different grid (3,15° > 1,7°). The average height of all
307 waves over the period (2015-2016) is 1.29 m and 9.30 m for the peak period. The analysis of the
308 different curves (**Figure 4**) of the wave parameters makes it possible to identify two phases: the
309 first going from June to July characterized by waves of fairly strong energy ($H_{smoy} > 1,32m$ and
310 $T_{pmoy} > 11s$). The second phase goes from July to August, it is characterized by slightly less
311 energetic waves ($H_{smoy} < 1,1m$ and $3,4s < T_p < 16s$). The wave periods during the first phase
312 are as high as the significant heights. In contrast, in the second phase, the wave height
313 decreased with the increase in wind speed [2]. The waves are therefore characterized by energy
314 spectra, which reveal characteristic quantities, with for example a significant height H_s , a
315 significant period T_s , etc.... These spectra are broad for wind waves, and narrower for an already
316 formed swell which continues to propagate far from its zone of generation by the wind.

317 ➤ In **Figures 5a, 5b**, it is noted that the calculated results for the depth water wave profile for
318 linear waves are quite similar to nonlinear waves, thus the comparisons indicate that the currently
319 obtained solutions deviate from the existing results of Cruz et al for regular linear waves, so some
320 anomaly is expected between the present results and Cruz's solutions formulated for nonlinear
321 waves. Water particle velocities under linear waves are greatest at the surface and decrease in
322 magnitude with depth (**Figures 5c** and **5d**). The speed of wave propagation depends on their
323 wavelength, their amplitude, and as they approach the coastline, the water depth (**Figures 5c**
324 and **5d**). The phenomenon of wave propagation is therefore dispersive. Furthermore, the waves do
325 not all propagate in the same direction, resulting in a sometimes chaotic appearance of the sea
326 surface state. The directions of particle speeds are linked to the movement of the water
327 surface. At the crest of the wave, the movement of the water is horizontal and in the direction of
328 the wave. At the trough, the speed is reversed (by the same magnitude as at the peak in linear
329 theory). Vertical velocities reach their maximum when water crossings occur. We notice that the
330 velocities of the water particles increase (**Figures 5c** and **5d**) and the accelerations of the water
331 particles decrease (**Figures 5e** and **5f**) from deep water to shallow water, this gives us a good
332 agreement between these results and previous results for deep-water and shallow-water wave
333 measurements. It can be said from the results obtained that the wave height has a considerable
334 effect on the wave profile. Then, the crest has moved, the pressure is maximum at its summit and
335 decreases going down in the direction of propagation (**Figure 5j**). The pressure decreases, so the
336 speed increases. On the other hand, in the left part of the direction of propagation, the pressure
337 increases from left to right (up to the trough), the pressure force acting under the wave crest is

338 greater than the pressure force under the wave trough leading to a net effort over a wave period
339 (Figure 5j). Figures 5a, 5b, 5c, 5d, 5e, 5f, 5g, 5h, show a good agreement between the speeds
340 and accelerations of the current model, there is only a difference in the values.

341 ➤ The analysis of the results, after several years of monitoring the morphodynamics of the
342 Beninese beach, made it possible to highlight the link between the sea surface and the
343 seabed. However, these results should be moderated due to the particularly favorable weather
344 conditions (absence of erosive storms) observed since 2011. In the breaking zone where $d = 3m$,
345 this potential also varies with a non-negligible average. The shoaling zone is therefore a zone of
346 strong amplification of the energy power of the swell, while those of Surf and Swash are the
347 zones of energy dissipation. These results show that the swells in Benin are more energetic in
348 the shoaling zone. The curves of Figures 6, 6a, and 6b, translate the variations of the vertical
349 elevation of the free surface of the ocean according to the local water depth. Note that the curve
350 of Figure 6 represents dimension 2 (2D) while those of Figures 6a and 6b are its representations
351 in dimension 3 (3D). They confirm:

- 352 - The constancy of the various offshore parameters.
- 353 - Height amplification crest to the trough of the swells in the shoaling zone under the
354 disturbing effect of the seabed.

355 The slope of this seabed causes the decrease or contraction of the wavelength. The curve of
356 Figure 6b, which represents the variations of the vertical elevation of the free surface of the
357 ocean according to the local water depth $d = \mu L_o$ and the slope of the seabed β in the shoaling
358 zone, reveals that the randomness accompanied by small oscillations on the surface of the swell
359 is due to the variability of the slope of the seabed.

360

361 4. CONCLUSION

362 In the Gulf of Guinea at Cotonou, the swells are regular and have a constant average
363 height $H_o = 0,8m$ and an average period $T = 11s$ in deep waters. In the coastal zone, the disturbing
364 effect of the seabed causes them to rise to the breaking point and it is the modified Boussinesq
365 theory, proposed by Peregrine in 1967, makes it possible to model them. These swells become
366 very energetic in this zone, their height is amplified and remains proportional to $(d^{-1/4})$. At the
367 breaking point, the maximum height these swells reach varies between $1,7m$ and $2,5m$. Their
368 bathymetric surge, occurs at a position where the local water depth d_b oscillates between $1.6m$
369 and $4.5m$ very close to the coastline depending on the value of the slope of the seabed. This
370 Breaking is a sudden energy discharge that induces and accentuates the phenomenon of coastal
371 erosion. The waves are therefore characterized by energy spectra, which reveal characteristic
372 quantities, with for example a significant height H_s , a significant period T_s , etc.... These spectra are
373 broad for wind waves, and narrower for an already-formed swell which continues to propagate far
374 from its zone of generation by the wind. Swells induce an orbital motion in the water and the
375 amplitude of this motion decreases with depth. It is important to note that the amplitude of the
376 velocity decreases exponentially with a coefficient proportional to the number of waves k . So, the
377 orbital velocity of swells with a longer period (smaller wave number) will be more present at sea
378 floor than that of waves with shorter periods. The propagation velocity of the swells depends on
379 their wavelength, their amplitude and when approaching the coast, the water depth. The swells
380 are therefore characterized by energy spectra, which show characteristic quantities, with for
381 example a significant height H_s , a significant period T_s , etc. Water particles also describe vertical
382 circles which become progressively smaller with increasing depth, the decrease being
383 exponential. The reason for describing simple waves is that they represent the basic solutions of
384 the physical equations that govern waves on the sea surface and they are the building blocks for
385 real wave fields occurring at sea. Actually, the idea of basic sinusoidal waves is widely applied to
386 help in the comprehension and characterization of waves. Despite this simplified description,
387 definitions and formulas derived from waves are intensively employed in practice and have
388 proven their value. It can be said from the results obtained that the wave height has a
389 considerable effect on the wave profile. It has a major impact on the wave and its constituent
390 parts, as seen by the fluctuation in water depth as a function of distance from the bed. From the

391 present work we can say that the combination of the effects of height and depth together
392 contribute to the understanding of the behavior of the wave and its velocities and accelerations of
393 the water particles. Therefore, the orbital speed of waves with a larger period (smaller number of
394 waves) will be more present at the bottom than that of waves with short periods. The speed of
395 wave propagation depends on their wavelength, their amplitude, and as they approach the coast,
396 the water depth. The phenomenon of wave propagation is therefore dispersive. Furthermore, the
397 waves do not all propagate in the same direction, resulting in a sometimes chaotic appearance of
398 the sea surface. The variation in the depth of the water as a function of the distance from the bed
399 shows that it has a very significant effect on the wave and its components. Wave propagation is a
400 phenomenon that is very sensitive to a large number of parameters, in particular, the speed of
401 the waves after breaking v_g , their period T , their wavelength in deep waters L_0 , the slope of the
402 seabed β , the crest to trough height of the swell H , the obliquity of the swell α , the local water
403 depth d . . .

404

405 **ACKNOWLEDGEMENTS**

406 The authors thank the Beninese Center for Scientific Research and Innovation
407 (IRHOB/CBRSI) not only for supporting this research work but also for the data made
408 available to us.

409

410 **AUTHORS CONTRIBUTIONS**

411 This work was carried out in collaboration between the author and all co-authors. "The main
412 author" and the "first three co-authors" designed the study, performed the statistical analysis, and
413 wrote the protocol and the first draft of the manuscript. The "last co-author" supervised and
414 coordinated the work. The other co-authors performed the calculations and analyses of the study.
415 All co-authors read and gave final approval for publication.

416

417 **CONFLICT OF INTEREST**

418 The authors state that there were no financial or commercial relationships that may be seen as
419 having a conflict of interest when conducting the research.

420

421 **DATA AVAILABILITY**

422 The datasets generated during and/or analyzed during the current study are available from the
423 authors at reasonable request.

424

425

426

426 **REFERENCES**

- 427 [1] N. B. TOKPOHOZIN, « INFLUENCE DE LA HOULE SUR LA DYNAMIQUE
428 SEDIMENTAIRE DANS LA ZONE CÔTIÈRE DU BENIN », Thèse de doctorat Unique,
429 Université d'Abomey-Calavi (UAC), Institut de Mathématiques et de Sciences Physiques
430 (IMSP), 2016.
- 431 [2] B. N. Tokpohozin *et al.*, « Prospects for the Characterization of the Fundamental
432 Parameters Linked to the Energy Spectrum of the Aeolian Sea State in Benin Coastal
433 Zone », *Curr. J. Appl. Sci. Technol.*, vol. 42, n° 42, p. 19-35, nov. 2023, doi:
434 10.9734/cjast/2023/v42i424270.
- 435 [3] Z. N. Al-Dwairi, K. Y. Tahboub, N. Z. Baba, C. J. Goodacre, et M. Özcan, « A Comparison
436 of the Surface Properties of CAD/CAM and Conventional Polymethylmethacrylate
437 (PMMA) », *J. Prosthodont.*, vol. 28, n° 4, p. 452-457, avr. 2019, doi: 10.1111/jopr.13033.
- 438 [4] G. Hervé Hounguè, B. B. Kounouhewa, R. Almar, Z. Sohou, J.-P. Lefebvre, et M.
439 Houépkonhéha, « Waves Forcing Climate on Bénin Coast, and the Link with Climatic Index,
440 Gulf of Guinea (West Africa) », *J. Coast. Res.*, vol. 81, n° sp1, p. 130, sept. 2018, doi:
441 10.2112/SI81-017.1.
- 442 [5] N. B. Tokpohozin, B. Kounouhewa, G. Y. H. Avossevou, A. Houekpoheham, et C. N.
443 Awanou, « Modelling of sediment movement in the surf and swash zones », *Acta Oceanol.*
444 *Sin.*, vol. 34, n° 2, p. 137-142, févr. 2015, doi: 10.1007/s13131-015-0610-2.

- 445 [6] R. Almar *et al.*, « The Grand Popo beach 2013 experiment, Benin, West Africa: from short
446 timescale processes to their integrated impact over long-term coastal evolution », *J. Coast.*
447 *Res.*, vol. 70, p. 651-656, avr. 2014, doi: 10.2112/SI70-110.1.
- 448 [7] O. G. Acclassato, N. B. Tokpohozin, C. D. Akowanou, A. M. Houékpoheha, G. H. Houngue,
449 et B. B. Kounouhéwa, « Study of Dissipating of Wave Energy in the Breakers Zone of the
450 Gulf of Guinea: Case of Autonomous Port of Cotonou in Benin Coastal Zone », *J. Mod.*
451 *Phys.*, vol. 13, n° 09, p. 1272-1286, 2022, doi: 10.4236/jmp.2022.139076.
- 452 [8] T. Noukpo Bernard, F. Jean-Louis C., H. H. Guy, H. A. Mathias, et K. B. Basile,
453 « ENERGETIC POWER ESTIMATION OF SWELLS AND ORBITAL MARINE CURRENTS
454 IN BENIN COASTAL ZONE (GULF OF GUINEA) », *Int. J. Adv. Res.*, vol. 11, n° 02, p.
455 366-382, févr. 2023, doi: 10.21474/IJAR01/16261.
- 456 [9] A. Melet, R. Almar, M. Hemer, G. Le Cozannet, B. Meyssignac, et P. Ruggiero,
457 « Contribution of Wave Setup to Projected Coastal Sea Level Changes », *J. Geophys. Res.*
458 *Oceans*, vol. 125, n° 8, p. e2020JC016078, août 2020, doi: 10.1029/2020JC016078.
- 459 [10] G. H. Houngue, M. A. Houékpoheha, N. B. Tokpohozin, et B. B. Kounouhéwa, « Wave
460 Energy Potential Assessment during Recent Extreme Events Observed on Benin's Coastal
461 Area, Gulf of Guinea (West Africa). », *Journal de physique de la SOAPHYS*, Afrique de
462 l'Ouest, p. 1 (2019) C19A15, 2019.
- 463 [11] G. H. Houngue, B. B. Kounouhéwa, M. A. Houékpoheha, B. N. Tokpohozin, et V. I.
464 Madogni, « Wave Energy Resources Assessment Offshore Benin from ERA Re-Analysis:
465 Gulf of Guinea », *Phys. Sci. Int. J.*, vol. 19, n° 4, p. 1-11, nov. 2018, doi:
466 10.9734/PSIJ/2018/44226.
- 467 [12] N. B. Tokpohozin, J.-L. Fannou, A. M. Houekpoheha, H. G. Houngue, et B. B.
468 Kounouhéwa, « STATISTICAL STUDY OF WAVE PARAMETERS : SEA STATES IN THE
469 DEEP WATERS (OFFSHORE) OF THE GULF OF GUINEA IN BENIN », *Int. J. Curr. Res.*,
470 vol. Vol. 15, n° Issue, 02, p. pp.23709-23719, févr. 2023, doi: 10.24941/ijcr.44701.02.2023.
- 471 [13] M. Rabaud et F. Moisy, « The Kelvin–Helmholtz instability, a useful model for wind-wave
472 generation? », *Comptes Rendus Mécanique*, vol. 348, n° 6-7, p. 489-500, nov. 2020, doi:
473 10.5802/crmeca.31.
- 474 [14] Aurélien BABARIT, Jean-Marc ROUSSET, Hakim MOUSLIM, Judicaël AUBRY, Hamid
475 BEN AHMED, et Bernard MULTON, « Chapter 4 Wave Prediction Models », in *Elsevier*
476 *Oceanography Series*, vol. 49, Elsevier, 1989, p. 75-105. doi: 10.1016/S0422-
477 9894(08)70124-7.
- 478 [15] M. Clauss, C. Nunn, J. Fritz, et J. Hummel, « Evidence for a tradeoff between retention time
479 and chewing efficiency in large mammalian herbivores », *Comp. Biochem. Physiol. A. Mol.*
480 *Integr. Physiol.*, vol. 154, n° 3, p. 376-382, nov. 2009, doi: 10.1016/j.cbpa.2009.07.016.
- 481 [16] D. Chalikov et D. Sheinin, « Modeling extreme waves based on equations of potential flow
482 with a free surface », *J. Comput. Phys.*, vol. 210, n° 1, p. 247-273, nov. 2005, doi:
483 10.1016/j.jcp.2005.04.008.
- 484 [17] D. Isebe *et al.*, « Une nouvelle approche pour la protection des plages : Application à la
485 plage du Lido de Sète », in *Xèmes Journées*, Sophia Antipolis, Editions Paralia, 2008, p.
486 263-272. doi: 10.5150/jngcg.2008.025-1.
- 487 [18] G. Chen, B. Chapron, R. Ezraty, et D. Vandemark, « A global view of swell and wind sea
488 climate in the ocean by satellite altimeter and scatterometer. », *Journal of atmospheric and*
489 *Oceanic Technology*, p. 1849-1859, 2002.
- 490 [19] Y. Xu et X. Yu, « Enhanced formulation of wind energy input into waves in developing
491 sea », *Prog. Oceanogr.*, vol. 186, p. 102376, juill. 2020, doi:
492 10.1016/j.pocean.2020.102376.
- 493 [20] J.-H. G. M. Alves, « Numerical modeling of ocean swell contributions to the global wind-
494 wave climate », *Ocean Model.*, vol. 11, n° 1-2, p. 98-122, janv. 2006, doi:
495 10.1016/j.ocemod.2004.11.007.
- 496 [21] G. M. A. Jose-Henrique, « Numerical modeling of ocean swell contributions to the global
497 wind-wave climate », *Ocean Modelling*, p. 98-122, 2006.

- 498 [22] B. Castelle, P. Bonneton, H. Dupuis, et N. Sénéchal, « Double bar beach dynamics on the
499 high-energy meso-macrotidal French Aquitanian Coast: A review », *Mar. Geol.*, vol. 245, n°
500 1-4, p. 141-159, nov. 2007, doi: 10.1016/j.margeo.2007.06.001.
- 501 [23] R. M. Castelao, « Mesoscale eddies in the South Atlantic Bight and the Gulf Stream
502 Recirculation region: Vertical structure », *J. Geophys. Res. Oceans*, vol. 119, n° 3, p.
503 2048-2065, mars 2014, doi: 10.1002/2014JC009796.
- 504 [24] Q. Liu *et al.*, « Observation-Based Source Terms in the Third-Generation Wave Model
505 WAVEWATCH III: Updates and Verification », *J. Phys. Oceanogr.*, vol. 49, n° 2, p.
506 489-517, févr. 2019, doi: 10.1175/JPO-D-18-0137.1.
- 507 [25] V. G. Polnikov, « The role of wind waves in dynamics of the air-sea interface », *Izv.*
508 *Atmospheric Ocean. Phys.*, vol. 45, n° 3, p. 346-356, juin 2009, doi:
509 10.1134/S0001433809030086.
- 510 [26] A. Zavadsky, D. Liberzon, et L. Shemer, « Statistical Analysis of the Spatial Evolution of the
511 Stationary Wind Wave Field », *J. Phys. Oceanogr.*, vol. 43, n° 1, p. 65-79, janv. 2013, doi:
512 10.1175/JPO-D-12-0103.1.
- 513